ChemComm

COMMUNICATION

View Article Online
View Journal | View Issue

Cite this: *Chem. Commun.*, 2022, **58**, 13963

Received 11th July 2022,
Accepted 21st November 2022

DOI: 10.1039/d2cc03862e

rsc.li/chemcomm

Optical and chemical control of the wettability of nanoporous photoswitchable films†

Zejun Zhang,[a] Donghui Chen,[a] Dragos Mutruc,[b] Stefan Hecht [bcd] and Lars Heinke *[a]

Wettability is a central surface property of functional thin films. Here, we present a nanoporous film made of an azobenzene-containing metal–organic framework material where the wettability is controlled by photoswitching of the fluorinated azobenzene moieties and by reversible incorporation of guest molecules with different polarities in the pores. Using both, the optical and the chemical stimuli, the water contact angle was modified over a wide range, from 23° to 97°.

Interfacial properties such as wettability are fundamental features of surfaces. Wettability is crucial for many processes in nature[1–3] and for many technical applications, such as the separations of emulsions.[4–6] The wettability of a given surface is typically evaluated by (static) contact angle measurements, where often water is used as a probe liquid.[6,7] The contact angle depends on the interfacial energy of the surface, the surface roughness and the heterogeneity.[8] While hydrophilic surfaces indicate favorable wetting with water contact angles of less than 90°, hydrophobic surfaces indicate unfavorable wetting with water contact angles greater than 90°.[6,7] By designing and structuring the surface, the contact angle can be adjusted.[9]

The dynamic control of the surface properties is highly desired for various applications, *e.g.*, in sensors, as lubricants and coatings.[3,10–12] Stimuli including pH-value changes, temperature and light are particularly interesting to externally control the wettability.[13–15] The major advantages of using light are its immediate, contact-less (and thus remote) and usually non-invasive nature – that in combination with photochromic molecules allows for reversible optical switching. So far, various surfaces based on photochromic molecules such as azobenzene and spiropyran have been presented which allow the remote control of the contact angle by light.[16,17] For example, azobenzene-terminated surfaces were presented where the contact angle is modified in the order of 10° by light-induced switching between the azobenzene *trans* and *cis* isomers.[18,19]

Metal–organic frameworks (MOFs) are a class of nanoporous crystalline materials. They are composed of metal ions and clusters, serving as (metal) nodes, connected by organic linker molecules.[20] Although most MOF materials are prepared in the form of crystalline powders, thin surface coatings of MOFs on solid substrates can also be prepared by various methods.[21,22] The wettability of the MOF surface is of great importance for applications in membrane-based oil-water separation and ion capture.[23,24] So far, numerous optically switchable MOF materials possessing photochromic molecules including azobenzenes, spiropyran and diarylethene have been presented where properties like the adsorption, diffusion, membrane separation and conduction are modulated.[25] The remote control of the wettability of a MOF surface has not yet been explored. While the embedment of guest molecules is a straightforward method to control the MOF properties, such as the electric[26,27] and thermal[28] conductivities or the chemical stability,[29] surface properties and wettability of MOFs have not yet been modulated by the guest loading.

Here, a nanoporous photoswitchable MOF thin film is presented where the wettability is controlled in a multi-stimuli way. This is realized by photoisomerization of parts of the MOF structure and by controlled guest loading in the pores. The MOF film has a pillared-layer structure, sketched in Fig. 1. The MOF possess photoswitchable *ortho*-fluorinated azobenzene side groups, that can reversibly be switched between their *trans* and *cis* configurations by violet and green light. By loading the nanoporous film with various guest molecules, here butanediol, octanol, and hexadecane, the polarity of the guest@MOF-film changes, shifting the water contact angle from

[a] *Karlsruhe Institute of Technology (KIT), Institute of Functional Interfaces (IFG), Hermann-von-Helmholtz-Platz 1, Eggenstein-Leopoldshafen, 76344, Germany. E-mail: Lars.Heinke@kit.edu*
[b] *Humboldt-Universität zu Berlin, Department of Chemistry & IRIS Adlershof, Brook-Taylor-Strasse 2, Berlin 12489, Germany*
[c] *DWI – Leibniz Institute for Interactive Materials, Forckenbeckstr. 50, Aachen 52074, Germany*
[d] *RWTH Aachen University, Institute of Technical and Macromolecular Chemistry, Worringer Weg 2, Aachen 52074, Germany*

† Electronic supplementary information (ESI) available. See DOI: https://doi.org/10.1039/d2cc03862e

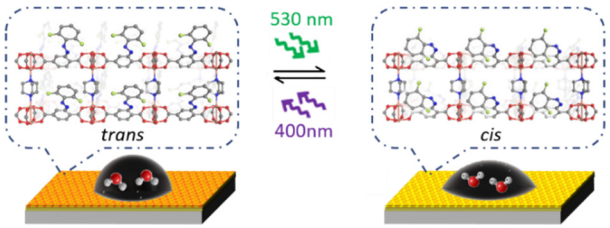

Fig. 1 $Cu_2(F_2AzoBDC)_2(dabco)$ structure in the *trans* form (left) and the *cis* form (right). The color code is: C grey, N blue, O red, F green, Cu orange and H is not shown. A sketch of the SURMOF thin film on the gold-coated Si-substrate with the water droplet on top is shown below.

$\sim 25^\circ$ to $\sim 100^\circ$. By *trans* → *cis* photoswitching of the azobenzene in the MOF structure, the water contact angle can be reversibly varied by additional 6–10°.

The $Cu_2(F_2AzoBDC)_2(dabco)$ MOF thin films were prepared on functionalized gold-coated silicon wafer substrates in a layer-by-layer (lbl) fashion, see ESI.† This lbl-MOF-synthesis results in surface-mounted MOFs, SURMOFs. The components of the SURMOF film are the Cu-dimer metal node, the (passive) dabco linker and the photoresponsive F_2AzoBDC linker. (dabco stands for 1,4-diazabicyclo[2.2.2]octane and F_2AzoBDC for (*E*)-2-((2,6-difluorophenyl)diazenyl)terephthalic acid.)

The crystallinity of the SURMOF film is explored by X-ray diffraction (XRD, Fig. 2a and Fig. S5, ESI†). The XRD data show that the SURMOF has a high crystallinity with the targeted structure. The out-of-plane XRD data show that the SURMOF samples are grown in the (001) orientation perpendicular to the substrate surface. The in-plane XRD data show the regular order of the MOF film parallel to the surface. The orientation of the film is also sketched in Fig. 1. The scanning electron microscopy (SEM) images of the sample are shown in Fig. 2c and d. The top-view SEM images show the SURMOF films have a regular morphology. The film is composed of many intergrown crystallites with a few small gaps in between and covers the entire substrate. The SEM images of the cross section of the SURMOF films were obtained from the broken samples, and a film thickness of ~1.2 μm was estimated.

The sample was further characterized by infrared-reflection-absorption spectroscopy (IRRAS) and energy-dispersive X-ray (EDX) spectroscopy and mapping, Fig. S2 and S3 (ESI†). The data from both techniques verify that the sample has the composition of the targeted $Cu_2(F_2AzoBDC)_2(dabco)$ structure.

The photoisomerization properties of the MOF film were explored by UV-vis spectroscopy, Fig. 2b. The sample was irradiated with green light of 530 nm and violet light of 400 nm, resulting in reversible changes in the UV-vis spectrum. The spectral changes can be correlated to green-light-induced *trans* → *cis* isomerization and violet-light-induced *cis* → *trans* isomerization of the azobenzene side groups,[30,31] see also Fig. 1. The photostationary state (PSS) was determined by infrared spectroscopy (Fig. S4, ESI†). Upon irradiation with green light, a PSS of 14% *trans* (and 86% *cis*, referred to as *cis* state) was determined. Upon violet light, 86% *trans* (and 14% *cis*, referred to as *trans* state) was determined. These PSS values are in agreement with previous studies.[32,33]

Atomic force microscopy shows that the morphology and surface roughness of the SURMOF is not affected by switching the azobenzene groups from *trans* to *cis*, Fig. S1 (ESI†). The surface roughness is ~10 nm. XRD show that the crystallinity is also not affected by the *trans*–*cis*-switching, Fig. S5 (ESI†).

For exploring the wettability of the SURMOF, we performed static contact angle measurements of water droplets under ambient conditions. The contact angle of the unloaded thin film is shown in Fig. 3. (We like to stress that there are most likely molecules from the environment, *e.g.* nitrogen and water

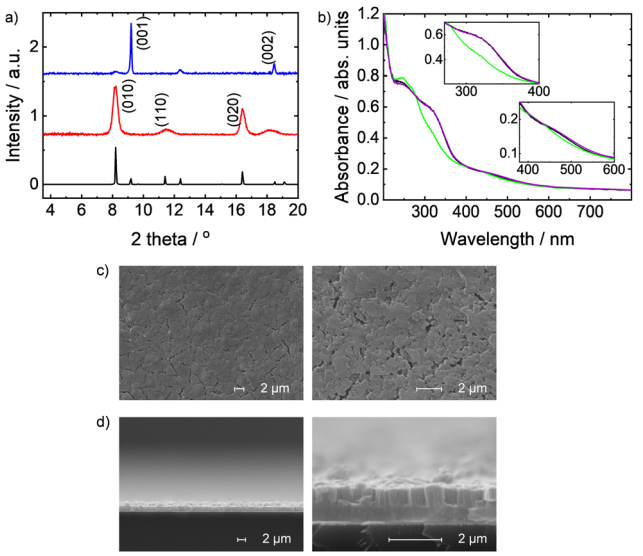

Fig. 2 (a) Out-of-plane (blue) and in-plane (red) XRDs of the SURMOF. For comparison, the calculated XRD of the targeted structure is shown in black. The X-ray wavelength is 0.154 nm. (b) UV-vis spectra of the SURMOF film in transmission mode. The black spectrum (widely covered by the violet spectrum) is from the thermally relaxed sample. The green and violet spectrum is from the sample upon green- and violet-light irradiation, respectively. The insets show zoom-ins. Scanning electron microscopy (SEM) images of (c) the top-view and (d) the cross section of the SURMOF film. The images have different magnifications and the scale bars are shown.

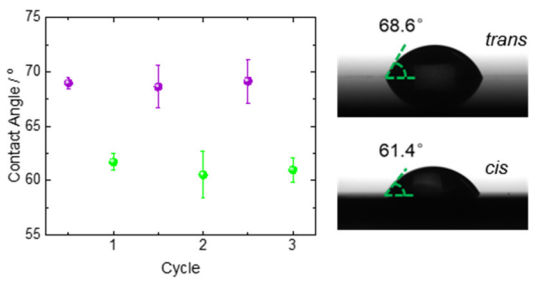

Fig. 3 The contact angle of water on the photoswitchable (unloaded) SURMOF. The violet spheres were obtained upon violet light irradiation (*trans*) and the green spheres upon green light (*cis*). The irradiation was performed for three cycles. For each point, the contact angle measurements were repeated three times at different positions on the sample and the average values with standard deviations are shown. Photographs of the water droplet on the sample in *trans* and *cis* are shown on the right-hand side. See also Fig. S8 (ESI†).

molecules, adsorbed in the MOF pores.) For the pristine sample, the average value of the water contact angle is 69°. Upon irradiation with green light, *i.e.* switching the SURMOF to the *cis* state, the contact angle decreases to 62°. By irradiation with violet light, which switches the sample back to the *trans* state, the contact angle changes back to its initial value of ~69°. Further irradiation with green or violet light results again in a contact angle of 62° or 69°, respectively. This means, by photoswitching the azobenzene side groups in the SURMOF, the wettability is reversibly modulated in a remote manner.

In addition to light, we explored the impact of the guest uptake by the nanoporous film as a further stimulus. To this end, we loaded the pores of the SURMOF film with 1,4-butanediol, *n*-hexadecane and 2-octanol, respectively. The molecules were chosen because of their size (allowing them to be loaded in the pores), their different polarity and their low vapor pressure (resulting in a very slow desorption from the pores). The molecules were loaded *via* the gas phase, avoiding liquid droplets on the surface, fully covering the SURMOF surface. (The XRD data of the loaded samples can be found in Fig. S6 (ESI†). The transient uptake data of the guests by the SURMOF are shown in Fig. S7, ESI†) For the butanediol-loaded SURMOF, the average value of the water contact angle drops to 23° for the sample in the *trans* state. Upon photoswitching to the *cis* state, the contact angle reversibly increases to ~29°, Fig. 4a. Upon loading the SURMOF film with octanol, the contact angle shifts to 75°. Then, the contact angle can be photoswitched between ~75° (*trans*) and ~65° (*cis*), Fig. 4b. Upon loading the sample with hexadecane, the contact angle is 97° in the *trans* state and can be reversibly photoswitched to 86°, Fig. 4c.

The contact angle data (see Fig. 3 and 4) show that the wettability can be modified over a wider range by filling the pores with different guest molecules. These guests are embedded in the pores and (most likely) only partially stick out of the external SURMOF surface. A clear trend is that a larger polarity results in a smaller contact angle. The dipole moments of *n*-hexadecane, *n*-octanol, and 1,4-butanediol are 0.06 D,[34] 1.69 D[35] and 2.58 D,[36] respectively, resulting in contact angles of 97°, 75° and 23°, respectively, for the loaded *trans*-SURMOFs. So, the wettability can be modified from highly hydrophilic (pores filled with butanediol), hydrophilic (unloaded or pores filled with octanol) to slightly hydrophobic (pores filled with hexadecane). The wettability of the sample with subsequent loadings is shown in Fig. S12 (ESI†).

Even more interesting, in all of the case, the contact angle was modified by *trans–cis*-switching the azobenzene side groups in the MOF structure. For the unloaded SURMOF, the *cis*-form is more hydrophilic than the *trans*-form and the contact angle can by modified by 6°. This can be explained by the changes of the polarity of the azobenzene moiety: while the *trans* isomer is essentially nonpolar, the *cis* isomer is polar with a dipole moment of ~3 D.[37,38] By loading the SURMOF pores with hexadecane and octanol, the finding that the *cis* form is more hydrophilic remains. Remarkably, compared to the unloaded SURMOF, the *trans–cis* difference substantially increases from ~6° to ~10°. There, the contact angle photoswitching is also

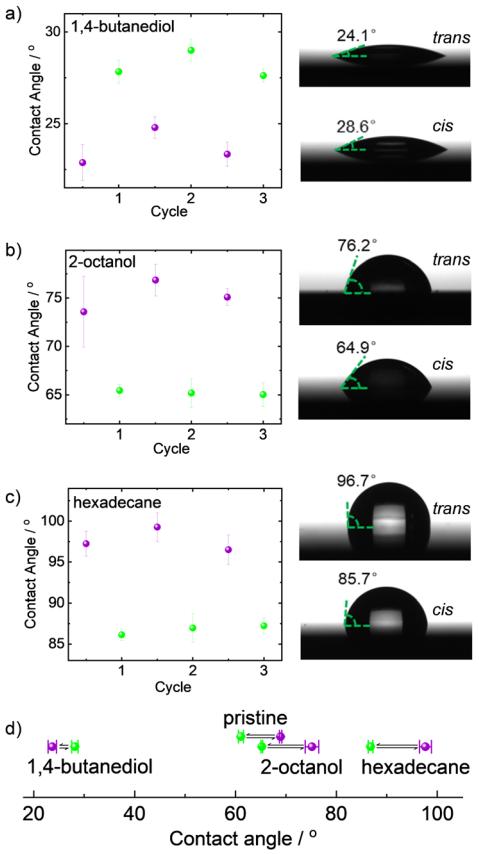

Fig. 4 The contact angle of water on the photoswitchable SURMOF loaded with (a) 1,4-butanediol, (b) 2-octanol and (c) hexadecane. The violet spheres were obtained upon violet light irradiation (*trans*) and the green spheres upon green light (*cis*). The irradiation was performed for three cycles. For each point, the contact angle measurements were repeated three times at different positions on the sample and the average values with standard deviations are shown. Photographs of the water droplet on the sample in *trans* (top) and *cis* (bottom) state are shown on the right-hand side. See also Fig. S9–S11 (ESI†). (d) The contact angle changes of the unloaded (pristine) and loaded SURMOF sample upon irradiation with green and violet light.

explained by the more polar *cis* azobenzene as compared to *trans*, causing a larger water wettability. Noteworthy, for hexadecane@SURMOF, the wettability is optically switched between slightly hydrophilic and hydrophobic.

Interestingly, the butanediol@SURMOF sample shows a higher contact for the *cis* form compared to *trans*. This can be well understood by the strong interaction between the OH-groups of butanediol and *cis* azobenzene, forming hydrogen bonds.[37] As a result, the polar *cis* azobenzene is shielded by butanediol, where the polar OH-groups point to the azobenzene. Then, the nonpolar carbon chain points out and interacts with water, increasing the contact angle. For the *trans*-SURMOF, there is no strong interaction with the butanediol guests and the butanediol OH groups cause a small water contact angle.

Generally, the amplitude of the contact-angle-change as result of SURMOF-photoswitching is similar to the contact-angle-switching of other azobenzene-terminated surfaces.[18,19] (It should be noted that somewhat larger contact

angle changes can be also realized by surfaces based on molecules with large polarity changes, such as spiropyran.[39,40]) Moreover, the combination with the guest-loading in the SURMOF provides a second stimulus which results in very large contact-angle changes, see Fig. 4d. Based on the stimuli-responsive contact-angle data and the correlation to other wettability measurements,[41,42] it can be assumed that the sliding angle and the advancing/receding angle are modulated in a similar way.

In summary, a nanoporous azobenzene-containing MOF thin film is presented where the wettability is controlled by embedment of different guests in the pores as well as by photoswitching of the functional moieties of the film. By using both stimuli, the water contact angle was reversibly modified between 23° and 97° in total. To the best of our knowledge, this is the first control of the contact angle by two different – an optical and a chemical – stimuli. The established multi-stimuli controlled wettability can be further extended, for example by exploring different photoswitches such as spiropyran with even larger changes of the dipole moment.[43,44] In the same way, different non-evaporating liquids, such as ionic liquids, can be embedded in the pores to adjust the contact angle.[45,46] The embedment of molecules responding to various stimuli, such as heat, pH, electrochemical potential,[13,14,47] should moreover enable the fabrication of MOF films with designed multi-responsive surface properties. Thus, we are convinced that this work will foster the development of smart surfaces with adjustable hydrophobic and hydrophilic properties.

We acknowledge funding through the Deutsche Forschungsgemeinschaft (DFG, *via* HE 7036/5, *via* SFB 951, project A3, and *via* SPP 1928) and the China Scholarship Council (CSC).

Conflicts of interest

There are no conflicts to declare.

Notes and references

1 V. Fernandez and M. Khayet, *Front. Plant Sci.*, 2015, **6**, 510.
2 A. K. Lenz, U. Bauer and G. D. Ruxton, *J. Exp. Bot.*, 2022, **73**, 1176–1189.
3 A. Solga, Z. Cerman, B. F. Striffler, M. Spaeth and W. Barthlott, *Bioinspiration Biomimetics*, 2007, **2**, S126–S134.
4 Q. L. Ma, H. F. Cheng, A. G. Fane, R. Wang and H. Zhang, *Small*, 2016, **12**, 2186–2202.
5 S. Agarwal, V. von Arnim, T. Stegmaier, H. Planck and A. Agarwal, *Sep. Purif. Technol.*, 2013, **107**, 19–25.
6 D. Ahmad, I. van den Boogaert, J. Miller, R. Presswell and H. Jouhara, *Energy Sources, Part A*, 2018, **40**, 2686–2725.
7 K. Y. Law, *J. Phys. Chem. Lett.*, 2014, **5**, 686–688.
8 Y. Yuan and T. R. Lee, *Surface science techniques*, Springer, 2013, pp. 3–34.
9 S. Riahi, B. Niroumand, A. D. Moghadam and P. K. Rohatgi, *Appl. Surf. Sci.*, 2018, **440**, 341–350.
10 S. Y. Leo, W. Zhang, Y. F. Zhang, Y. L. Ni, H. Jiang, C. Jones, P. Jiang, V. Basile and C. Taylor, *Small*, 2018, **14**, 10.
11 Z. Dang, L. B. Liu, Y. Li, Y. Xiang and G. L. Guo, *ACS Appl. Mater. Interfaces*, 2016, **8**, 31281–31288.
12 A. J. J. Kragt, D. J. Broer and A. Schenning, *Adv. Funct. Mater.*, 2018, **28**, 7.
13 H. Mahani, R. Menezes, S. Berg, A. Fadili, R. Nasralla, D. Voskov and V. Joekar-Niasar, *Energy Fuels*, 2017, **31**, 7839–7853.
14 P. Escale, L. Rubatat, C. Derail, M. Save and L. Billon, *Macromol. Rapid Commun.*, 2011, **32**, 1072–1076.
15 D. Kessler, F. D. Jochum, J. Choi, K. Char and P. Theato, *ACS Appl. Mater. Interfaces*, 2011, **3**, 124–128.
16 C. Y. Zong, M. Hu, U. Azhar, X. Chen, Y. B. Zhang, S. X. Zhang and C. H. Lu, *ACS Appl. Mater. Interfaces*, 2019, **11**, 25436–25444.
17 N. Wagner and P. Theato, *Polymer*, 2014, **55**, 3436–3453.
18 N. Delorme, J. F. Bardeau, A. Bulou and F. Poncin-Epaillard, *Langmuir*, 2005, **21**, 12278–12282.
19 X. W. Pei, A. Fernandes, B. Mathy, X. Laloyaux, B. Nysten, O. Riant and A. M. Jonas, *Langmuir*, 2011, **27**, 9403–9412.
20 O. M. Yaghi, M. J. Kalmutzki and C. S. Diercks, *Introduction to Reticular Chemistry: Metal-Organic Frameworks and Covalent Organic Frameworks*, Wiley, 2019.
21 P. Falcaro, R. Ricco, C. M. Doherty, K. Liang, A. J. Hill and M. J. Styles, *Chem. Soc. Rev.*, 2014, **43**, 5513–5560.
22 L. Heinke and C. Wöll, *Adv. Mater.*, 2019, **31**, 1806324.
23 Z. W. Long, L. H. Yuan, J. Y. Chen, L. Luo, C. Shi, C. Q. Wu, H. Qiao and K. L. Wang, *Adv. Mater. Interfaces*, 2022, **9**, 2102427.
24 A. Mähringer, M. Hennemann, T. Clark, T. Bein and D. D. Medina, *Angew. Chem., Int. Ed.*, 2021, **60**, 5519–5526.
25 F. Bigdeli, C. T. Lollar, A. Morsali and H.-C. Zhou, *Angew. Chem., Int. Ed.*, 2020, **59**, 4652–4669.
26 A. A. Talin, A. Centrone, A. C. Ford, M. E. Foster, V. Stavila, P. Haney, R. A. Kinney, V. Szalai, F. El Gabaly, H. P. Yoon, F. Leonard and M. D. Allendorf, *Science*, 2014, **343**, 66–69.
27 A. Dragasser, O. Shekhah, O. Zybaylo, C. Shen, M. Buck, C. Woll and D. Schlettwein, *Chem. Commun.*, 2012, **48**, 663–665.
28 H. Babaei, M. E. DeCoster, M. Jeong, Z. M. Hassan, T. Islamoglu, H. Baumgart, A. J. H. McGaughey, E. Redel, O. K. Farha, P. E. Hopkins, J. A. Malen and C. E. Wilmer, *Nat. Commun.*, 2020, **11**, 4010.
29 Y.-H. Shih, Y.-C. Kuo, S. Lirio, K.-Y. Wang, C.-H. Lin and H.-Y. Huang, *Chem. – Eur. J.*, 2017, **23**, 42–46.
30 C. Knie, M. Utecht, F. L. Zhao, H. Kulla, S. Kovalenko, A. M. Brouwer, P. Saalfrank, S. Hecht and D. Bleger, *Chem. – Eur. J.*, 2014, **20**, 16492–16501.
31 D. Bleger, J. Schwarz, A. M. Brouwer and S. Hecht, *J. Am. Chem. Soc.*, 2012, **134**, 20597–20600.
32 K. Müller, A. Knebel, F. Zhao, D. Bléger, J. Caro and L. Heinke, *Chem. – Eur. J.*, 2017, **23**, 5434–5438.
33 A. B. Kanj, J. Bürck, N. Vankova, C. Li, D. Mutruc, A. Chandresh, S. Hecht, T. Heine and L. Heinke, *J. Am. Chem. Soc.*, 2021, **143**, 7059–7068.
34 A. V. Astin, Standard Materials, National Bureau of Standards, 1962.
35 Z. Wang, U. Wille and E. Juaristi, *Encyclopedia of Physical Organic Chemistry, 6 Volume Set*, Wiley, 2017.
36 Z. B. Wang, S. Grosjean, S. Brase and L. Heinke, *ChemPhysChem*, 2015, **16**, 3779–3783.
37 K. Müller, J. Helfferich, F. L. Zhao, R. Verma, A. B. Kanj, V. Meded, D. Bléger, W. Wenzel and L. Heinke, *Adv. Mater.*, 2018, **30**, 1706551.
38 H. M. D. Bandara and S. C. Burdette, *Chem. Soc. Rev.*, 2012, **41**, 1809–1825.
39 R. Rosario, D. Gust, M. Hayes, F. Jahnke, J. Springer and A. A. Garcia, *Langmuir*, 2002, **18**, 8062–8069.
40 D. Dattilo, L. Armelao, G. Fois, G. Mistura and M. Maggini, *Langmuir*, 2007, **23**, 12945–12950.
41 M. Miwa, A. Nakajima, A. Fujishima, K. Hashimoto and T. Watanabe, *Langmuir*, 2000, **16**, 5754–5760.
42 E. Pierce, F. J. Carmona and A. Amirfazli, *Colloids Surf., A*, 2008, **323**, 73–82.
43 H. A. Schwartz, S. Olthof, D. Schaniel, K. Meerholz and U. Ruschewitz, *Inorg. Chem.*, 2017, **56**, 13100–13110.
44 A. B. Kanj, A. Chandresh, A. Gerwien, S. Grosjean, S. Bräse, Y. Wang, H. Dube and L. Heinke, *Chem. Sci.*, 2020, **11**, 1404–1410.
45 K. Fujie and H. Kitagawa, *Coord. Chem. Rev.*, 2016, **307**, 382–390.
46 A. B. Kanj, R. Verma, M. Liu, J. Helfferich, W. Wenzel and L. Heinke, *Nano Lett.*, 2019, **19**, 2114–2120.
47 J. Elbert, M. Gallei, C. Ruttiger, A. Brunsen, H. Didzoleit, B. Stuhn and M. Rehahn, *Organometallics*, 2013, **32**, 5873–5878.

